Hindawi
Advances in Materials Science and Engineering
Volume 2017, Article ID 8308612, 9 pages
https://doi.org/10.1155/2017/8308612

*Research Article*

# The Influence of the Activation Temperature on the Structural Properties of the Activated Carbon Xerogels and Their Electrochemical Performance

**Nguyen Khanh Nguyen Quach,[1] Wein-Duo Yang,[1] Zen-Ja Chung,[2] and Hoai Lam Tran[3]**

[1]*Department of Chemical and Materials Engineering, National Kaohsiung University of Applied Sciences, 415 Chien-Kung Road, Kaohsiung 807, Taiwan*
[2]*Chemical Engineering Division, Institute of Nuclear Energy Research, Lungtan, Taoyuan 325, Taiwan*
[3]*Department of Chemical Technology, Ho Chi Minh City University of Food Industry, Tan Phu, Ho Chi Minh 700000, Vietnam*

Correspondence should be addressed to Wein-Duo Yang; ywd@kuas.edu.tw

Received 6 March 2017; Revised 5 July 2017; Accepted 16 July 2017; Published 13 August 2017

Academic Editor: Andrea Lamberti



The effect of activation temperature on the structural properties and the electrochemical performance of KOH-activated carbon xerogel was investigated in range of 700 to 1000°C. At a high temperature (1000°C), the chemical activation regenerated a more crystalline network structure of activated carbon xerogels, which was observed by Raman, XRD, and TEM images. Additionally, SEM images, BET, BJH, and *t*-plot were used to study the structural properties of carbon xerogels. The carbon xerogel sample activated at 900°C was found with the most appropriate structure, which has the high micropore area and a more-balanced porosity between the micropores and mesopores, for using as an electrode material. The highest obtained specific capacitance value was 270 $Fg^{-1}$ in 6 M KOH electrolyte at scan rate of 5 $mVs^{-1}$ from the cyclic voltammetry.

## 1. Introduction

In recent years, the utilization of acid catalysts in the preparation process of carbon xerogels has received much research attention by scientists because of a significant shortening effect of the preparation process, which leads to a decrease of the cost of products. Moreover, acid-catalyzed carbon xerogels also have excellent properties such as low density, high electrical conductivity, high surface area, and large pore volume [1], which are appropriate for applications as adsorbents, as porous electrodes for supercapacitors.

However, further improvement of the characteristic properties of carbon xerogels is necessary to enhance their application efficiency, especially for use as an electrode material in electrical double-layer capacitors. The activation route is suggested to improve the structural properties of carbon xerogels by generating carbon materials with higher porosity is the chemical activation, which is a process of heating the mixture and includes the impregnation of an activating reagent onto a carbon precursor, resulting in greater development of a porous structure [2–4]. The temperatures used in this case are lower than used in the other activation process.

In addition, the compatibility between the structural properties and the electrolyte ion size also plays an important role, which contributes to enhancing the electrochemical performance of carbon xerogel electrodes [5–7]. Therefore, investigation into the control of pore size in the carbon structure so that the pore size is small enough to have the highest surface area but also large enough for the pore size to approach the electrolyte ion size or find of the most appropriate electrolyte for the pore size of the generated carbon samples was suggested.

In this work, we reported a simple method for the preparation of a carbon xerogel and subsequent activation with KOH to generate activated carbon xerogels. The effect of the activation temperature on the characteristic properties of carbon xerogels was investigated to determine the optimal preparation conditions of the carbon xerogels and activated

carbon xerogels. The electrochemical performance of the carbon xerogel and activated carbon xerogel electrodes was also studied in both inorganic and organic electrolytes to seek the most appropriate electrolyte solution to the structural properties of carbon xerogels and activated carbon xerogels for use as electrode materials in electrical double-layer capacitors.

## 2. Experimental Methods

*2.1. Carbon Xerogel and Activated Carbon Xerogel Synthesis.* After preliminary investigations, organic xerogels were prepared by condensation of 0.1 mol of resorcinol in 15 ml of water and 0.2 mol of formaldehyde, with 2.86 ml of glacial acetic acid added as a catalyst. The mixtures were stirred for 30 minutes, poured into the glass vials, and placed in an oven at 80°C for 3 days to obtain the gel. The wet gels were washed with acetone for 2 days and then dried by subcritical drying for 1 day at 100°C to generate the organic xerogels. Carbon xerogels were prepared by pyrolysis of the organic gels at 800°C under nitrogen for 3 h with using a tube furnace. The resultant carbon xerogels were mixed with KOH at a weight ratio of 1 : 4 for activation in the same tube furnace under nitrogen in the temperature range from 700 to 1000°C for 1 h with a heating ramp rate of 3°C $min^{-1}$. The resultant activated carbon xerogels were washed with distilled water until the pH value of solution reached approximately 7 and then were dried in an oven at 120°C for 3 h. Carbon xerogels and activated carbon xerogels were denoted as CX and ACX-*T*, where *T* is the activation temperature in the range from 700 to 1000°C.

*2.2. Characterization.* The BET surface area, BJH mesopore area, *t*-Plot micropore area, and $N_2$ adsorption-desorption isotherms were measured with a Micrometrics ASAP 2020 instrument. A JOEL microscope (model JSM 6330 TF) was used for the structural characterization. The crystallinity was investigated with using the Analytical Scanning Transmission Electron Microscope (model JEOL TEM-3010). X-ray diffraction patterns were detected with a Bruker D8 advance using Cu K$\alpha$ radiation. Raman spectra were obtained with a Raman spectroscopy (HORIBA, HR550).

*2.3. Electrochemical Properties*

*Fabrication of the Electrodes of CX and ACX-T.* A mixture of CX or each of ACX-*T* and polytetrafluoroethylene as a binder and black carbon as a conductive additive with weight ratio of 8 : 1 : 1 was dispersed in 2-propanol and then ultrasonicated for 30 minutes to generate a homogeneous mixture. The resultant slurry was coated onto graphite paper as a current collector.

*Electrochemical properties* were investigated using a conventional three-electrode cell system by cyclic voltammetry and charge/discharge galvanostatic method. Cyclic voltammetry measurements was carried out at scan rate from 5 to 100 mV $s^{-1}$ in 1 M $H_2SO_4$ within a voltage range from −0.3 to 0.4 V, in 6 M KOH within a voltage range from −1.0 to 0 V, and in 1 M $TEABF_4$/ACN within a voltage range from −0.6 to 1.4 V. Charge/discharge galvanostatic measurements were performed at constant current of 1 and 5 $Ag^{-1}$ in 6 M KOH within the same voltage range as the cyclic voltammetry measurements.

Table 1: Characteristic properties of carbon xerogels and activated carbon xerogels.

| Name | $S_{tot}$ $m^2$ $g^{-1}$ | $S_{micro}$ $m^2$ $g^{-1}$ | $V_{tot}$ $cm^3$ $g^{-1}$ | Average pore size nm |
|---|---|---|---|---|
| CX | 578 | 390 | 0.97 | 6.72 |
| ACX-700 | 1115 | 818 | 1.27 | 4.54 |
| ACX-800 | 1247 | 886 | 1.40 | 4.48 |
| ACX-900 | 1750 | 893 | 1.91 | 4.37 |
| ACX-1000 | 2152 | 315 | 2.65 | 4.93 |

## 3. Result and Discussion

*3.1. Characterization of the Material.* All organic xerogels prepared in this study were monolithic and homogeneous samples with low densities and the preparation process with glacial acetic acid catalyst made the gelation process occur within 1 to 2 hours due to the growth mechanism under acid catalysis [8]. The porosity and surface properties of a carbon xerogel (CX) and activated carbon xerogels (ACXs) were investigated by nitrogen sorption analysis. The nitrogen adsorption-desorption isotherms, the pore volume, and pore size distribution of the CX and ACXs are shown in Figure 1. Their BET surface area, micropore surface area, pore volume, and pore size are listed in Table 1.

All samples show type IV isotherms with an H2 type hysteresis loop and the average pore size is less than 50 nm, which is characteristic of well-developed micro-/mesoporous structures. The ACX samples show greater development in porous structure, compared to that of CX sample; hence the BET surface area of the ACX samples shows higher value than that of CX sample; it maybe affirms that chemical activation with KOH causes the improvement in the specific surface area and total pore volume of carbon xerogel with the smaller pore size due to greater development in the porous structure. Moreover, increasing the activation temperature leads to increasing the capacity of producing the narrow micropores and widening the preexisting micropores by KOH and thus the porosity of ACX increases with increasing the activation temperature, which can be observed in Figure 1(a). So, the BET surface area and pore volume of ACXs increase with increasing activation temperature in the range from 700 to 1000°C. However, the preexisting micropore widening process or the transformation of micropores to mesopores in the carbon material was accelerated at high activation temperature due to the increase of the melting speed of $K_2CO_3$ and $K_2O$ as well as the evaporating speed of K during the activation process at high temperature [9]. The acceleration of this process was found at an activation temperature of 1000°C. This can be also observed in Figure 1(a) with a much greater loop of ACX-1000 sample and the pore size in range from 2 to 50 nm, which is characteristic of mesoporous material due

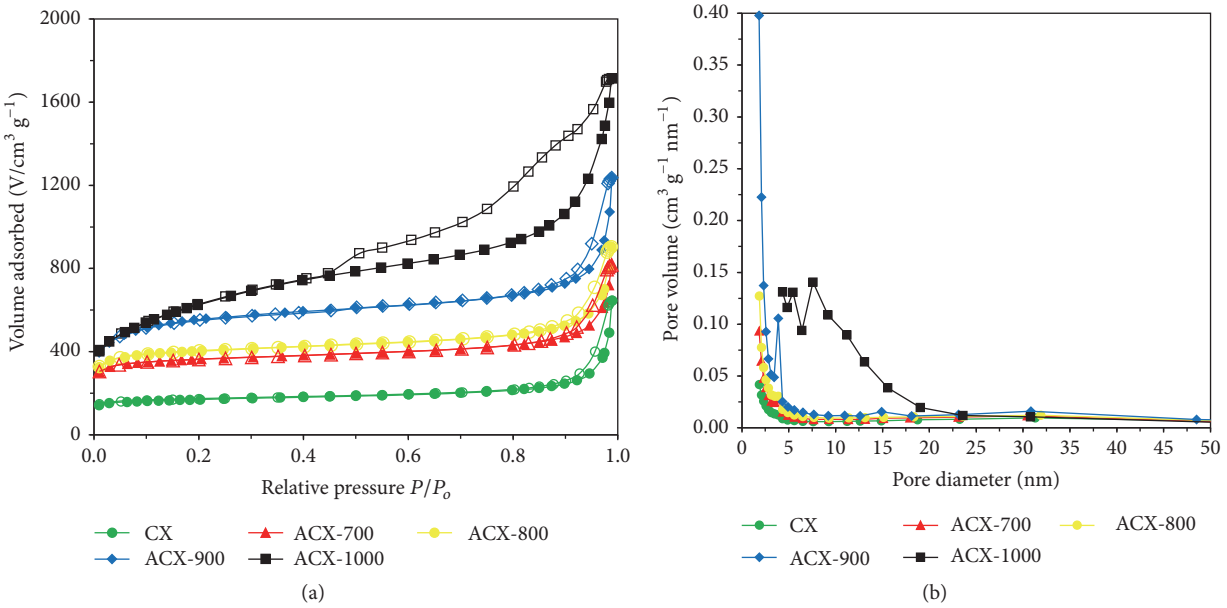


Figure 1: Nitrogen adsorption-desorption isotherms (a) and pore size distributions (b) of carbon xerogel and activated carbon xerogels.

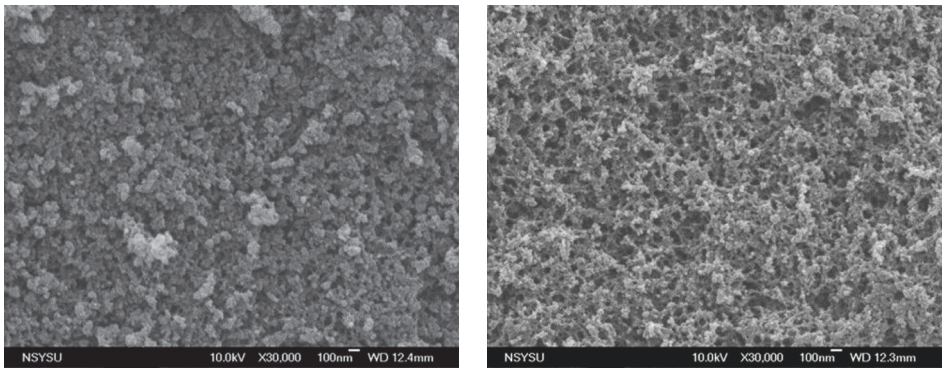


(a) (b)

Figure 2: SEM images of (a) carbon xerogel CX and (b) activated carbon xerogel ACX-900.

to capillary condensation. Therefore, the ACX-1000 sample had the highest BET surface area of 2152 $m^2 g^{-1}$ with the high mesoporous surface area and the largest pore volume of 2.64 $cm^3 g^{-1}$. The ACX-900 sample had more-balanced porosity between the micropores and mesopores with the highest micropore area of 893 $m^2 g^{-1}$.

The development in the porous structure of ACXs was shown by the SEM images (Figure 2). The morphology of the ACX-900 sample (Figure 2(b)) shows a denser network structure with smaller interconnected particles, resulting in enhanced surface area and pore volume compared to carbon xerogel before activation (Figure 2(a)), which was consistent with the BET results listed in Table 1.

Figure 3 shows the Raman spectra of CX and ACXs. The peak positions and intensity ratio of the D-band to G-band are listed in Table 2. All samples exhibited two characteristic peaks of graphite: the G-band near 1590 $cm^{-1}$ with $E_{2g}$ symmetry assigned to ordered carbon and the D-band near 1343 $cm^{-1}$ with $A_{1g}$ symmetry, which is forbidden in perfect graphite and is assigned to disorder [10]. Consequently, the transfer of the peak position of the G-band in ACXs to lower wavenumber compared to that in CX and the larger intensity ratio $I_D/I_G$ of ACXs than that of CX are caused by chemical activation procedure with KOH, resulting in various defects in the carbon structure. The intensity ratio of the activated carbon xerogels increases with increasing activation temperature; however, there was a slight decrease of the intensity ratio and change in the peak position of the G-band of the ACX-1000 sample compared to the other ACXs due to rearrangement in the lamellas of the carbon crystallite when carbon material was treated under severe activation conditions.

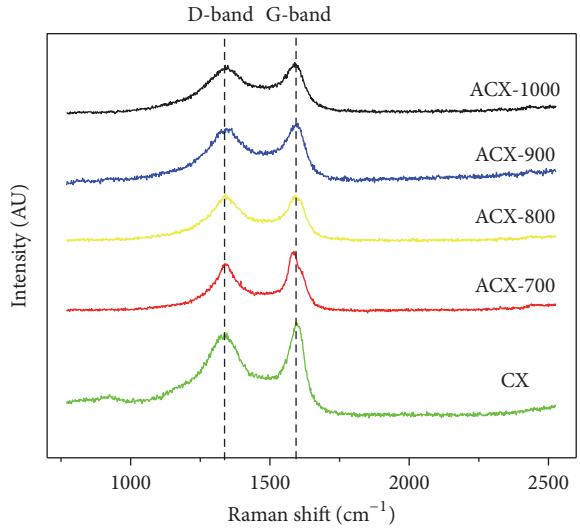


Figure 3: Raman spectra of CX, ACX-700, ACX-800, ACX-900, and ACX-1000.

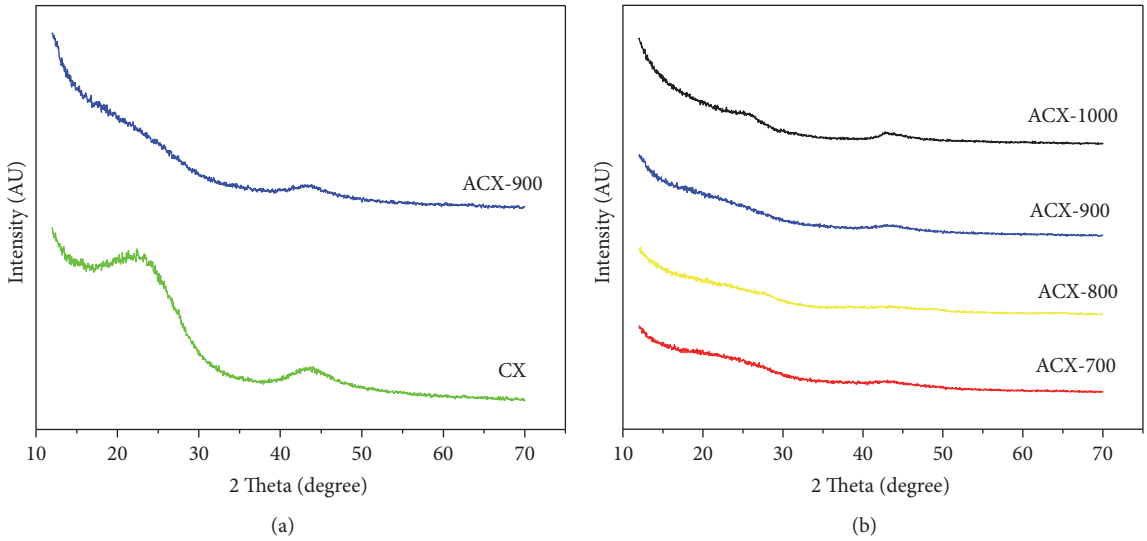


Figure 4: XRD patterns of (a) CX and ACX-900 and (b) ACX-700, ACX-800, ACX-900, and ACX-1000.

Table 2: Peak position and intensity ratio of the D-band with respect to the G-band ($R = I_D/I_G$) of CX and ACX-$T$.

| Name | D-band | G-band | $R$ ($I_D/I_G$) |
|---|---|---|---|
| CX | 1345 | 1592 | 0.903 |
| ACX-700 | 1343 | 1589 | 0.969 |
| ACX-800 | 1343 | 1589 | 0.988 |
| ACX-900 | 1341 | 1589 | 1.002 |
| ACX-1000 | 1345 | 1590 | 0.939 |

In addition, the graphitization of the CX and ACXs was investigated by X-ray diffraction. The XRD patterns of the CX and ACX-900 samples are displayed in Figure 4(a). Two diffraction peaks of (002) and (101) of the CX reflections correspond to the graphitic phase of carbon [11]. The XRD pattern of ACX-900 was partly different from that of CX; the (002) peak of the ACX-900 sample was broadened. Moreover, when increasing the activation temperature the (002) peak intensity of ACXs decreases (Figure 4(b)), which indicates that various defects and loss of hexagonal symmetry occurred on the surface of the ACX samples upon chemical activation with KOH. However, the two peak intensities of (002) and (101) of ACX-1000 sample were higher than those of the other ACXs, indicating a more crystalline network structure of ACX-1000 sample compared to the other activated carbon xerogels, which is in good agreement with the Raman spectra results. This rearrangement of the carbon crystallite of

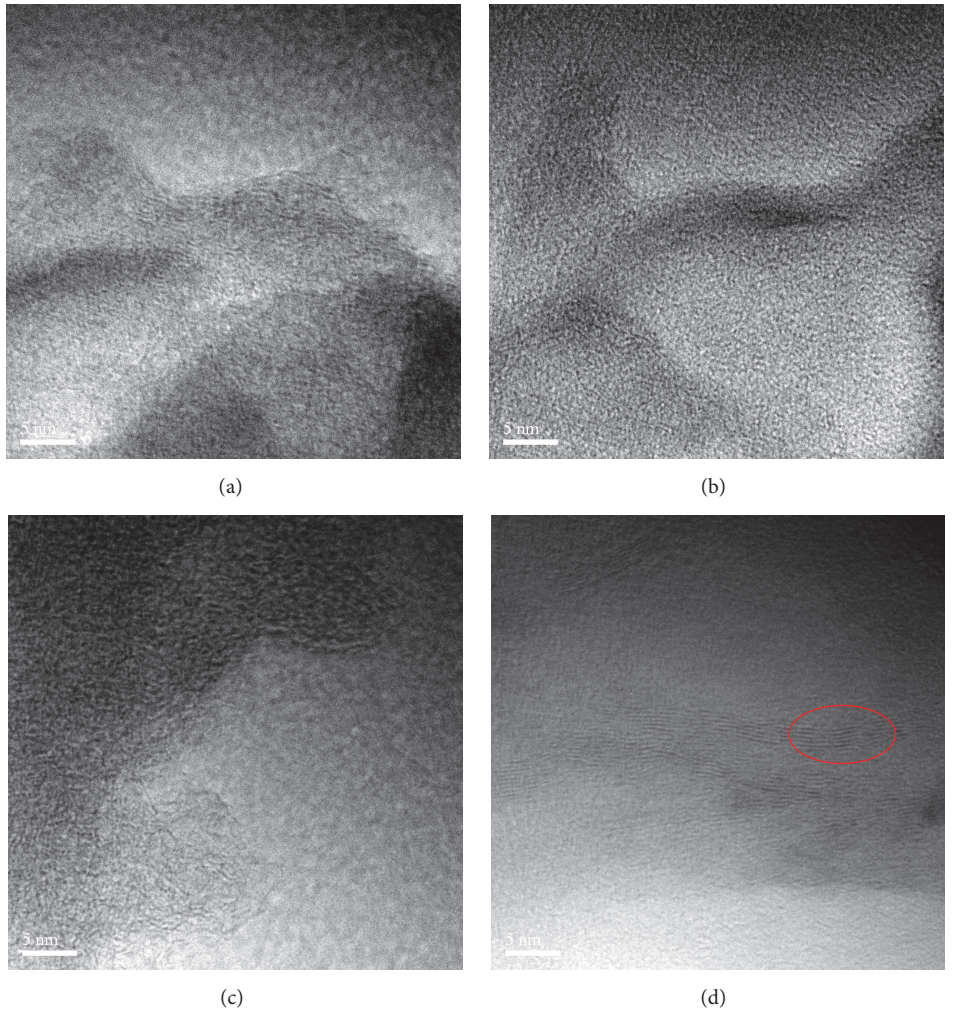


Figure 5: TEM images of activated carbon xerogel ACX-700 (a), ACX-800 (b), ACX-900 (c), and ACX-1000 (d).

ACX-1000 sample is observed more clearly by TEM images shown in Figure 5. Figure 5(d) show a more crystalline network structure compared with the others TEM images.

*3.2. Electrochemical Properties.* The electrochemical properties of the CX and ACX electrodes were investigated in both inorganic and organic electrolyte solutions. Figure 6 shows the cyclic voltammograms of the carbon xerogel and activated carbon xerogel electrodes in 1 M $H_2SO_4$, 6 M KOH, and 1 M $TEABF_4$/ACN electrolyte solutions. The specific capacitance values of the CX and ACX electrodes were calculated over the voltage range from −1 to 0 V in 6 M KOH, from −0.3 to 0.4 V in 1 M $H_2SO_4$, and from −0.6 to 1.4 V in 1 M $TEABF_4$/ACN using the integrated total charge density [12]. The calculated specific capacitances of the CX and ACX-900 electrodes in 1 M $H_2SO_4$, 6 M KOH, and 1 M $TEABF_4$/ACN electrolytes at a scan rate of 10 $mVs^{-1}$ are listed in Table 3.

All of the carbon electrodes had the electrochemical behavior in both inorganic and organic electrolyte solutions. The electrodes operated in organic electrolyte with a larger potential window of 2 V compared to a maximum of 1 V in the inorganic electrolytes; this voltage limitation is imposed by electrolyte decomposition on the active surface of carbon [13]. Nevertheless, the CX and ACX electrodes obtained higher specific capacitance in the inorganic electrolytes and reached the highest specific capacitance in 6 M KOH because the diffusivity of organic electrolyte ions into the micropores of the carbon electrodes is smaller than that of the inorganic electrolyte ions due to the compatibility of the electrolyte ion size with the pore size of the carbon material [4, 5]. The pore size of a carbon material must approach the electrolyte ion size to maximize the amount of electrolyte ions accumulated into the micropores of the carbon electrodes, which resulted in an increased electrochemical performance of the carbon xerogel electrodes. Therefore, the detailed investigation of the electrochemical performance of all carbon xerogel electrodes in 6 M KOH electrolyte was performed.

Figures 6(c) and 6(d) shows the cyclic voltammograms of the carbon xerogel and activated carbon xerogel electrodes at scan rates of 10 to 100 $mVs^{-1}$. All cyclic voltammograms of carbon xerogel and activated carbon xerogel electrodes

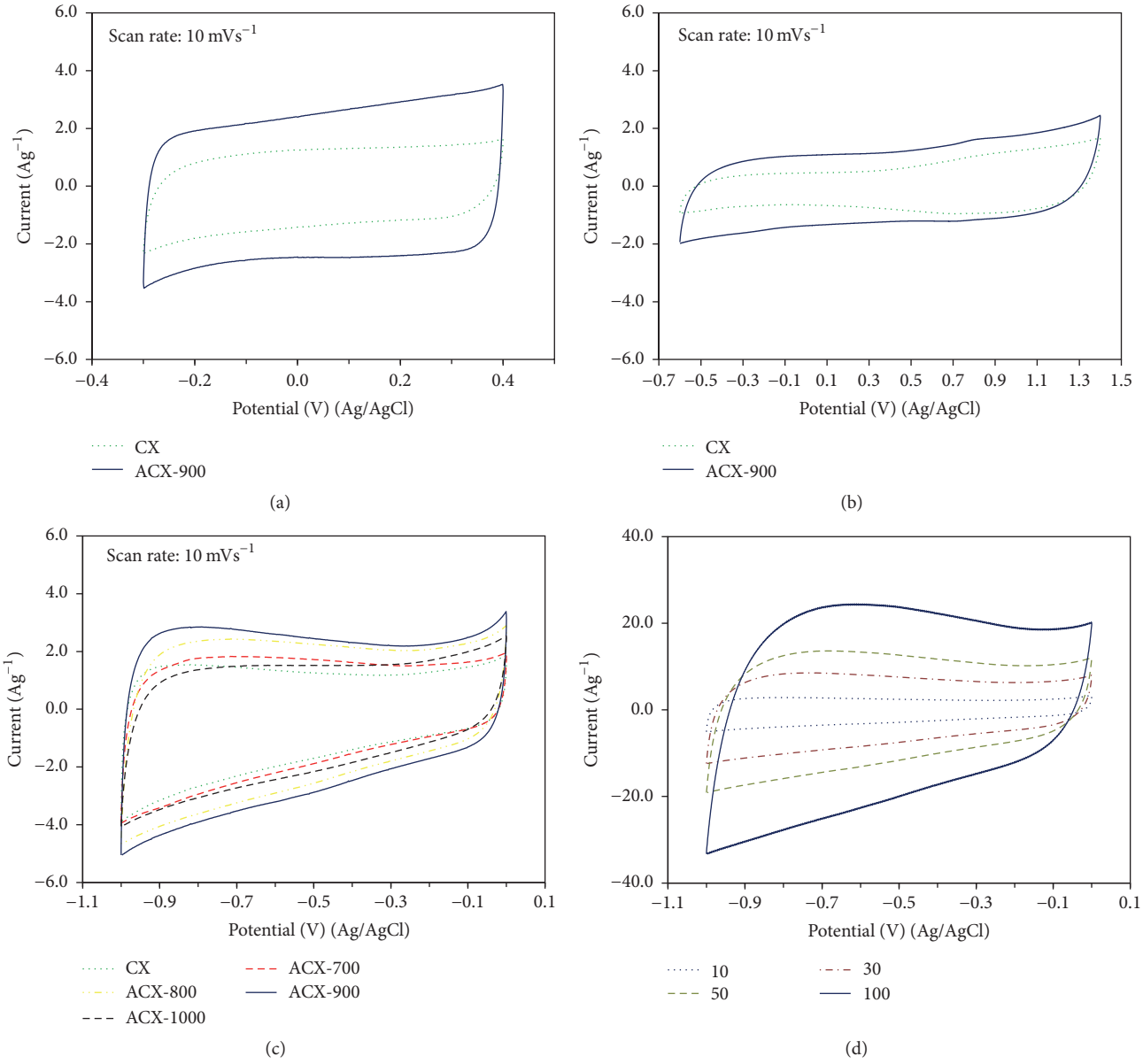


Figure 6: Cyclic voltammograms of CX and ACX electrodes at scan rates of 10 mVs$^{-1}$ (a) in 1 M $H_2SO_4$; (b) in 1 M $TEABF_4$/ACN; (c) in 6 M KOH electrolyte solutions and (d) cyclic voltammograms of ACX-900 electrode at various scan rates from 10 to 100 mVs$^{-1}$.

Table 3: Specific capacitance of the CX and ACX-900 electrodes in inorganic and organic electrolytes determined by cyclic voltammetry at a scan rate of 10 mVs$^{-1}$.

| Sample | Specific capacitance/Fg$^{-1}$ | | |
|---|---|---|---|
| | $H_2SO_4$, 1 M | KOH, 6 M | $TEABF_4$/ACN, 1 M |
| CX | 123 | 156 | 80 |
| ACX-900 | 245 | 263 | 127 |

at scan rates of 10 mVs$^{-1}$ (Figure 6(c)) have similar rectangular shape. After increasing the scan rates to 50 mVs$^{-1}$ (Figure 6(d)), the cyclic voltammograms of the ACX-900 electrode maintained an approximate rectangular shape. These results indicate that all carbon electrodes prepared in this study retain the general electrochemical performance of carbon material, and they have stable electrochemical performance at a high scan rate in a 6 M KOH electrolyte. At a higher scan rate of 100 mVs$^{-1}$, the cyclic voltammograms of the ACX-900 electrode was distorted due to the decrease in the ion transfer rate in the electrolyte, which reduced the specific capacitance. The calculated specific capacitances of the CX and ACX electrodes at various scan rates of 5 to 100 mVs$^{-1}$ are listed in Table 4.

The specific capacitance values of the ACX electrodes are higher than that of the CX electrode, indicating that the chemical activation with KOH affected not only the characteristic properties of the carbon xerogel but also their

Table 4: Specific capacitance of the CX and ACX electrodes in 6 M KOH electrolyte determined by cyclic voltammetry at various scan rates of 5 to 100 $mVs^{-1}$.

| Sample | Specific capacitance/$Fg^{-1}$ | | | | |
|---|---|---|---|---|---|
| | 5 $mVs^{-1}$ | 10 $mVs^{-1}$ | 30 $mVs^{-1}$ | 50 $mVs^{-1}$ | 100 $mVs^{-1}$ |
| CX | 169 | 156 | 138 | 128 | 109 |
| ACX-700 | 190 | 177 | 146 | 132 | 115 |
| ACX-800 | 245 | 227 | 191 | 170 | 135 |
| ACX-900 | 270 | 263 | 232 | 217 | 185 |
| ACX-1000 | 190 | 173 | 144 | 130 | 112 |

Table 5: Specific capacitance of the CX and ACX electrodes in 6 M KOH electrolyte obtained by the charge/discharge galvanostatic measurements at current densities 1 $Ag^{-1}$ and 5 $Ag^{-1}$.

| Sample | Specific capacitance/$Fg^{-1}$ | |
|---|---|---|
| | 1 $Ag^{-1}$ | 5 $Ag^{-1}$ |
| CX | 159 | 119 |
| ACX-700 | 178 | 129 |
| ACX-800 | 186 | 135 |
| ACX-900 | 204 | 153 |
| ACX-1000 | 161 | 120 |

electrochemical performance. The specific capacitance values of the ACX electrodes showed a conical shape with respect to the activation temperature: the highest specific capacitance of 270 $Fg^{-1}$ was obtained by the ACX-900 electrode at a scan rate of 5 $mVs^{-1}$. The specific capacitance value of ACX-1000 decreased suddenly. The electrochemical properties of the ACX-900 electrode are improved significantly compared with the activated carbon aerogel [14] with a similar specific surface area value but with a mainly microporous structure, which is prepared by the more complicated drying in vacuum. These results are due to the difference in the structural properties of the ACX-900 sample with the highest micropore area and a more-balanced porosity between the micropores and mesopores from that of other samples. Mesopores make the electrolyte ion adsorption into the micropores easier, and these electrolyte ions were transferred to the micropores, which improved the electrochemical performance by maximizing the charge accumulation [15, 16]. In addition to the compatibility of the electrolyte ion size and the pore size, the structural properties with high micropore surface area and well-balanced porosity between micropores and mesopores of the carbon xerogel material also play an important role in enhancing their electrochemical performance.

Moreover, the electrochemical performance of the CX and ACX electrodes in both inorganic and organic electrolyte solutions was also investigated by charge/discharge galvanostatic measurement at current densities of 1 $Ag^{-1}$ and 5 $Ag^{-1}$. Figure 7 shows the charge/discharge curve of the CX and ACX electrodes in both inorganic and organic electrolyte solutions (Figures 7(a), 7(b), and 7(c)) and the Coulombic efficiency of ACX-900 electrodes in 6 M KOH electrolyte for 2000 cycles (Figure 7(d)). The specific capacitance values of the CX and ACX electrodes were obtained from the charge/discharge galvanostatic using integration of the discharge curve [17] and were listed in Table 5.

The charge/discharge curves of all electrodes exhibited a triangular shape, demonstrating that the electrodes have capacitive behavior. The deviation in the charge/discharge curves of carbon xerogel electrodes at low current density could be due to the structural properties as well as the dispersion of the particles, resulting in the different rates of adsorption and desorption of electrolyte ions [18, 19]. In 6 M KOH electrolyte solution (Figures 7(a) and 7(b)) the ACX electrodes had longer charge/discharge time than the CX electrode, and the ACX-900 electrode exhibited the longest charge/discharge time, which resulted in higher specific capacitance of the ACX electrodes compared to that of the CX electrode. The ACX-900 electrode reached an excellent specific capacitance of 204 $Fg^{-1}$ at current density 1 $Ag^{-1}$ in 6 M KOH electrolyte solution. Besides, the Coulombic efficiencies of ACX-900 electrode also showed the highest value of 96% after 2000 cycles in 6 M KOH (in Figure 7(d)) compared to that in the other electrolyte solutions. These results are in good agreement with the cyclic voltammetry result.

## 4. Conclusions

Carbon xerogels were prepared by simple route using drying under ambient pressure and subsequently they were activated by KOH. The utilization of glacial acetic acid as the catalyst shortened significantly the gelation time, which contributes to reducing the product cost. The chemical activation with KOH improved the carbon xerogel properties significantly. On the effect of the activated temperature the structural properties of activated carbon xerogels were investigated in large range from mainly microporous to micro-/mesoporous structure, which is appropriate for many different applications, in which the carbon xerogel activated at 900°C showed the best electrochemical performance for being used as an electrode material with a high specific capacitance of 270 $Fg^{-1}$ at a scan rate of 5 $mVs^{-1}$ based on the cyclic voltammetry because of its suitable structural properties with a well-balanced porosity between the micropores and mesopores and the highest micropore surface area, which played important roles in enhancing the electrochemical performance of the carbon materials. Besides, the regeneration of a more crystalline network structure of the activated carbon xerogel was found when the activation temperature was increased

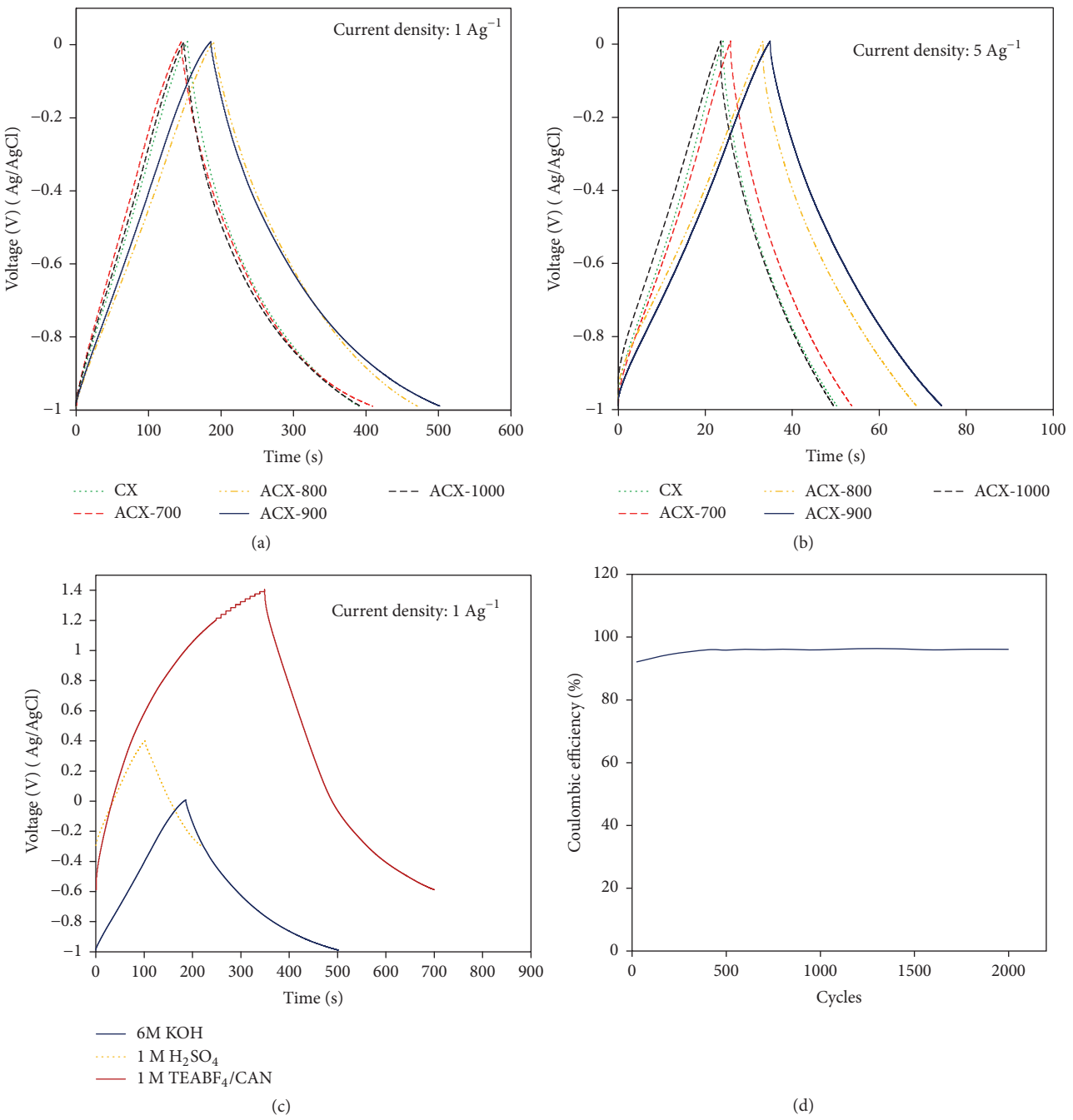


Figure 7: Charge/discharge curve of the CX and ACX electrodes at current densities of (a) 1 $Ag^{-1}$ and (b) 5 $Ag^{-1}$ in 6 M KOH electrolyte solution; of ACX-900 electrode at current densities of 1 $Ag^{-1}$ in all electrolyte solutions (c) and its Coulombic efficiency (d).

to 1000°C that was demonstrated by changes in the peak position of G-band and the $I_D/I_G$ ratio of the Raman spectra as well as the intensity and width of the X-ray diffraction peak.

## Conflicts of Interest

The authors declare that they have no direct financial relation with the commercial identities mentioned in this paper that might lead to conflicts of interest for any of them.

## Acknowledgments

The authors would like to thank the Ministry of Science and Technology of Taiwan for its financial support of this work (Grant no. MOST 103-2221-E-151-055).

## References

[1] R. Saliger, V. Bock, R. Petricevic, T. Tillotson, S. Geis, and J. Fricke, "Carbon aerogels from dilute catalysis of resorcinol with

formaldehyde," *Journal of Non-Crystalline Solids*, vol. 221, no. 2-3, pp. 144–150, 1997.

[2] S. H. Kwon, E. Lee, B.-S. Kim et al., "Activated carbon aerogel as electrode material for coin-type EDLC cell in organic electrolyte," *Current Applied Physics*, vol. 14, no. 4, pp. 603–607, 2014.

[3] Y. J. Lee, G.-P. Kim, Y. Bang, J. Yi, J. G. Seo, and I. K. Song, "Activated carbon aerogel containing graphene as electrode material for supercapacitor," *Materials Research Bulletin*, vol. 50, pp. 240–245, 2014.

[4] H. Chen, F. Wang, S. Tong, S. Guo, and X. Pan, "Porous carbon with tailored pore size for electric double layer capacitors application," *Applied Surface Science*, vol. 258, no. 16, pp. 6097–6102, 2012.

[5] J. Chmiola, G. Yushin, Y. Gogotsi, C. Portet, P. Simon, and P. L. Taberna, "Anomalous increase in carbon at pore sizes less than 1 nanometer," *Science*, vol. 313, no. 5794, pp. 1760–1763, 2006.

[6] E. Raymundo-Piñero, K. Kierzek, J. Machnikowski, and F. Béguin, "Relationship between the nanoporous texture of activated carbons and their capacitance properties in different electrolytes," *Carbon*, vol. 44, no. 12, pp. 2498–2507, 2006.

[7] J. Eskusson, P. Rauwel, J. Nerut, and A. Jänes, "A hybrid capacitor based on Fe3O4-graphene nanocomposite/few-layer graphene in different aqueous electrolytes," *Journal of the Electrochemical Society*, vol. 163, no. 13, pp. A2768–A2775, 2016.

[8] M. Sudhir and S.-L. Chariklia, *Materials and Processing: Organic – Natural and Synthetic, Aerogels Handbook*, Springer, New York, NY, USA, 1st edition, 2011, p. 215.

[9] Z. Shen and R. Xue, "Preparation of activated mesocarbon microbeads with high mesopore content," *Fuel Processing Technology*, vol. 84, no. 1-3, pp. 95–103, 2003.

[10] C. Ferrari and J. Robertson, *Phys. Riv. B*, vol. 61, p. 14095, 2000.

[11] S. Mitani, S.-I. Lee, K. Saito, Y. Korai, and I. Mochida, "Contrast structure and EDLC performances of activated spherical carbons with medium and large surface areas," *Electrochimica Acta*, vol. 51, no. 25, pp. 5487–5493, 2006.

[12] T. Thomberg, T. Tooming, T. Romann, R. Palm, A. Janes, and E. Lust, *J. Electrochem. Soc*, vol. 160, p. 1834, 2013.

[13] P. Azaïs, L. Duclaux, P. Florian et al., "Causes of supercapacitors ageing in organic electrolyte," *Journal of Power Sources*, vol. 171, no. 2, pp. 1046–1053, 2007.

[14] Q. N. K. Nguyen, "Wein-Duo Yang and Zen-Ja Chung," *Mater. Res. Innov*, vol. 19, p. 172, 2015.

[15] C. Vix-Guterl, E. Frackowiak, K. Jurewicz, M. Friebe, J. Parmentier, and F. Béguin, "Electrochemical energy storage in ordered porous carbon materials," *Carbon*, vol. 43, no. 6, pp. 1293–1302, 2005.

[16] G. Salitra, A. Soffer, L. Eliad, Y. Cohen, and D. Aurbach, "Carbon electrodes for double-layer capacitors. I. Relations between ion and pore dimensions," *Journal of the Electrochemical Society*, vol. 147, no. 7, pp. 2486–2493, 2000.

[17] E. Tee, I. Tallo, T. Thomberg, A. J, and E. Lust, *J. Electrochem. Soc*, vol. 163, p. 1317, 2016.

[18] C. Zequine, C. K. Ranaweera, Z. Wang et al., "High-Performance Flexible Supercapacitors obtained via Recycled Jute: Bio-Waste to Energy Storage Approach," *Scientific Reports*, vol. 7, no. 1, 2017.

[19] H. Yoo, G. Heo, and S. Park, "Effect of crystallinity on the electrochemical properties of carbon black electrodes," *Carbon Letters*, vol. 12, no. 4, pp. 252–255, 2011.